Check for updates

Substituting fossil-based with bio-based chemicals: the case of limonene as a greener pore expander for micellar templated silica†

Umair Sultan, [ab] Katrin Städtke,[a] Andreas Göpfert,[a] Daniel Lemmen,[a] Ezzeldin Metwali,[c] Santanu Maiti,[c] Carola Schlumberger,[d] Tadahiro Yokosawa,[e] Benjamin Apeleo Zubiri,[e] Erdmann Spiecker,[e] Nicolas Vogel,[b] Tobias Unruh,[c] Matthias Thommes[d] and Alexandra Inayat[a]

Porous materials are widely used in applications such as adsorption, catalysis and separation. The use of expander molecules is a versatile route to enlarge the mesopore size in micellar templated mesoporous silica materials. Typical expanders used for this purpose are fossil-based organic molecules such as trimethylbenzene (TMB). In the course of making such syntheses greener and more sustainable, it is highly desirable to substitute such fossil-based chemicals with renewable ones. Here, we show that bio-based limonene can be used as an alternative expander molecule for the synthesis of large-pore templated silica. On the basis of electron microscopy, nitrogen physisorption and small angle X-ray scattering we show that the substitution of TMB by limonene leads to very similar material characteristics, reaching mean mesopore diameters of 17–19 nm. A comparative life-cycle assessment demonstrates the reduced environmental impact of limonene production from citrus peel waste compared to TMB production, supporting the call for more applications of renewable chemicals, ideally from waste-streams, also for the production of porous materials.

Sustainability spotlight

One route to approach the UN SDGs 12 (Responsible Consumption and Production) and 13 (Climate Action) is the substitution of fossil-based by renewable feedstocks for the production of chemicals and materials. The need for such substitution also impacts the preparation of porous materials, which constitute a large group of materials with widespread industrial and daily-life application. Our case study on micellar templated porous silica shows that the substitution of a fossil-based by a bio-based chemical can lead to similar or even improved material properties while enhancing the overall greenness of the production process, which is evident from a comparative life cycle assessment (LCA). Our LCA considers the whole production chain of both chemicals and calculates the related environmental impacts. Based on different LCA scenarios we demonstrate the environmental advantages of using renewable energy (addressing SDGs 7 and 13), a waste material rather than a directly grown feedstock for the production of the bio-based chemical and the importance of a sustainable agriculture to further reduce biomass-related impacts (SDG 12).

[a]Institute of Chemical Reaction Engineering, Department of Chemical and Biological Engineering, Friedrich-Alexander Universität Erlangen-Nürnberg, Egerlandstrasse 3, 91058 Erlangen, Germany. E-mail: alexandra.inayat@fau.de

[b]Institute of Particle Technology, Department of Chemical and Biological Engineering, Friedrich-Alexander-Universität Erlangen-Nürnberg, Cauerstrasse 4, 91058 Erlangen, Germany

[c]Institute for Crystallography and Structural Physics (ICSP), Department of Physics, Friedrich-Alexander Universität Erlangen-Nürnberg, Staudtstrasse 3, Erlangen 91058, Germany

[d]Institute of Separation Science and Technology, Department of Chemical and Biological Engineering, Friedrich-Alexander-Universität Erlangen-Nürnberg, Egerlandstrasse 3, 91058, Erlangen, Germany

[e]Institute of Micro- and Nanostructure Research (IMN), Center for Nanoanalysis and Electron Microscopy (CENEM), IZNF, Friedrich-Alexander-Universität Erlangen-Nürnberg, IZNF, Cauerstrasse 3, 91058 Erlangen, Germany

† Electronic supplementary information (ESI) available: Low magnification SEM images, additional pore size distribution curves and micropore volume for all samples, parameters used for data simulation together with the life cycle inventory details for life cycle assessment. See DOI: https://doi.org/10.1039/d3su00068k. The raw and meta data files for all the measurements/analytical results presented in this article are available at: https://doi.org/10.5281/zenodo.8158744

Introduction

The development of greener synthesis approaches is a vital element of making the production of chemicals and materials more sustainable, *e.g.*, by reducing harmful emissions, stopping the depletion of non-renewable raw materials and integrating anthropogenic production processes into natural material cycles.[1,2]

Porous materials are a large group of materials that directly or indirectly impact our daily life, from washing powder, thickeners in paints, auxiliaries in pharmaceutical production and car exhaust gas catalysts up to the little silica gel sachets we often find in new shoes and electronic equipment to control humidity. Among these, micellar templated silica (MTS, often also named ordered mesoporous silica) constitutes a large class of mesoporous materials with amorphous silica walls surrounding a defined mesopore system.[3] MTS materials have

wide-spread industrial applications and potential applications as catalyst supports,[4] *e.g.*, for enzymes,[5,6] Keggin ions,[7] and for biorefinery-related conversions,[8] chromatography column materials and metal extraction,[3] drug delivery matrixes,[9] gas adsorption and storage,[10] and many other processes requiring large interfaces and pore volumes accessible also for larger (*e.g.*, bio-based) molecules. Their synthesis requires a silica source, a solvent (typically water), acids or bases to adjust the pH, and organic substances to template and tailor the defined mesopore system for their specific applications.[3]

The pore diameter of MTS materials like Santa Barbara Amorphous-15 (SBA-15, cylindrical mesopores) is typically in the range of 5–10 nm, under certain synthesis conditions even 15 nm.[11] With the help of expander molecules (swelling agents) this pore diameter can be increased further as illustrated in Fig. 1. If the expander amount exceeds a certain expander to mesopore template ratio then the well-ordered pore alignment (*e.g.*, hexagonal in the case of SBA-15) is lost and can transform towards a spherical, mesocellular foam-like pore structure with cell sizes in the range of 22–42 nm and pore entrances of 8–23 nm.[12,13]

The prevalent expander molecule for MTS syntheses, in the presence of cationic[14] and also neutral surfactants like poloxamers (*e.g.*, Pluronic P123), is trimethyl benzene.[13] Also, *n*-octane,[15] toluene,[16,17] xylenes, ethylbenzene, toluene, cyclohexane and 1,3,5-triisopropyl benzene[7,18,19] have been reported for pore expansion.

Many of the substances involved in MTS synthesis are still fossil-based, corrosive or even hazardous, but greening efforts are already underway and emerge as a growing research direction in the preparation of porous materials.[20] For example, the phospholipid lecithin,[21] alkylglycosides,[22,23] palmitic acid,[24] tannic acid,[25] oleylamines,[26] gelatine,[27] and yeast-derived sophorolipids[28] were successfully applied as bio-based mesopore templates. Some of these templates such as tannic acid and gelatine were reported to also increase the pore size of the obtained materials. In another greening approach, the use of strong acids (typically HCl) and post-synthetic neutralisation washes in SBA-15 synthesis were avoided by a novel UV-light based radical method to control silica condensation.[29]

An unexplored approach for greener MTS synthesis is the substitution of the above-mentioned, all fossil-based expander molecules (micelle swelling agents) by bio-based, *i.e.*, renewable ones. Accordingly, this contribution extends the choice of renewable expander molecules and presents a study on substituting the conventional fossil-based expander molecule TMB with the bio-based molecule limonene. Limonene is a cyclic monoterpene (Fig. 2) with lemon-like smell, yellow colour and wide use, *e.g.*, as a bio-based solvent and fragrance in commodities like shower gel and soap.[30] With 95% it is the main constituent of citrus peel oil[31] but is also present in turpentine oil and can be obtained *via* isomerisation of pinene, which is the main constituent of turpentine oil (a by-product of the wood and paper industry).[32] Accordingly, limonene is currently mainly produced from upcycled waste streams of the food and paper industry, making its use very desirable in respect to a more efficient raw material consumption and waste prevention,[2] which is in line with the UN SDG 12 (Responsible Consumption and Production). Limonene does not belong to the group of substances of very high concern,[33] which is an important precondition for the exploitation of any chemical towards more sustainable production processes.[34] From a material synthesis point of view, we found limonene interesting as a bio-based alternative to TMB and other aromatic/
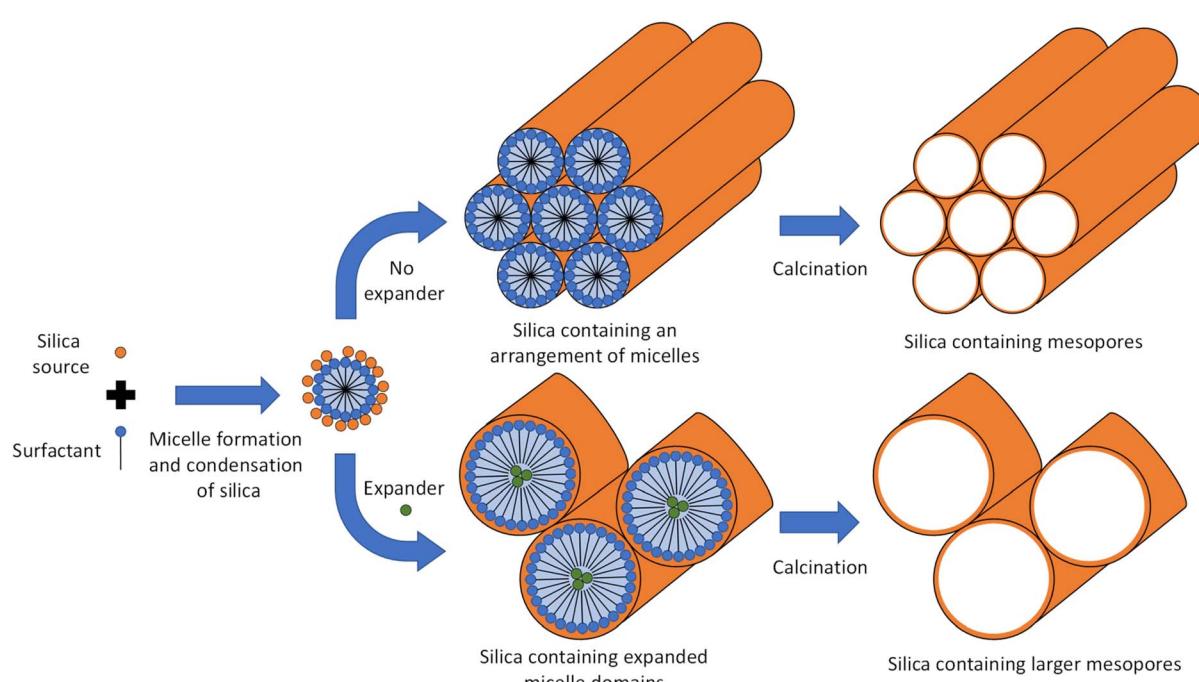

Fig. 1   Schematic illustration of the expander action in micellar templated silica.

     © 2023 The Author(s). Published by the Royal Society of Chemistry
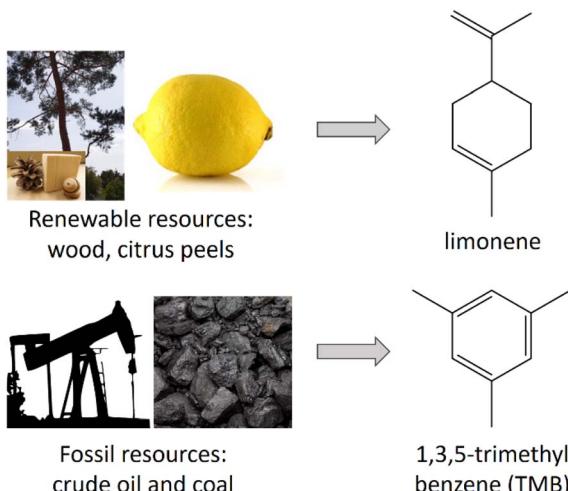
Fig. 2 Current raw materials and molecular structure of TMB and limonene, which were investigated as expander molecules for micellar templated silica in the present study.

cyclic expander molecules in MTS synthesis because it has a comparable composition and molecular structure (Fig. 2) and therefore, would potentially interact in a similar manner with the mesopore template Pluronic P123 (polyethylene polypropylene triblock copolymer).

In the second part of this contribution the results of the life cycle assessment are presented, which we conducted to clarify if the substitution of TMB by limonene is not only greener by fulfilling one of the twelve green chemistry principles (*i.e.*, use of renewable materials)[35] but more importantly if it also has less environmental impacts considering the whole production chain from raw materials sourcing up to expander production.

Results and discussion

Comparative characterisation of mesoporous silica obtained using different amounts of limonene and TMB as expanders

To compare the pore expanding effect of limonene and TMB we conducted silica syntheses with increasing amounts of both expander molecules using the triblock co-polymer Pluronic P123 as the templating agent. The textural data of the resulting materials (pore size distribution, pore volume, specific surface area) were determined from nitrogen physisorption isotherms which are shown in Fig. 3a and c. All isotherms are of type IVa,[36] indicating the presence of mesopores in the material. An increase in total adsorbed volume is observed as the amount of added expander is increased. The total adsorbed volume is an indication of the volume of mesopores inside the material. As can be seen from Table 1, similar amounts of TMB and limonene, respectively, lead to similar total pore volume. Furthermore, an increasing expander amount results in a shift of the hysteresis loop in the isotherms to higher relative pressure values, which indicates an increase of the average pore size. This increase is also visible in the pore size distribution curves (Fig. 3b and d). The broadening of the pore size distribution curves with increasing expander amount can be explained with

an increasing deviation of the number of expander molecules which are integrated in the growing P123 micelles. However, the pore size distribution is still narrower and the mesopores have larger volume compared to non-templated silica gel (see Fig. S1†), *i.e.*, the use of template and expander is still needed to create the textural properties also in the case of large-pore MTS material like LIM-36. Moreover, for all samples the adsorption and desorption branches of each isotherm (Fig. 3a and c) run parallel to each other and with narrow distance resulting in an H1 hysteresis.[36] Such a shape of the hysteresis loop in the isotherms indicates that the pore morphology is predominantly cylindrical with the majority of pores being freely accessible and not restricted by narrower pore windows.[37,38] This is also indicated by the good agreement of the pore size distributions determined from the adsorption branch using a cylindrical metastable Non-linear Density Function Theory (NLDFT) kernel and the pore size distributions calculated from the desorption branch using a cylindrical equilibrium NLDFT kernel (Fig. S2†). This interpretation is further supported by the TEM images in Fig. 4, where we see that syntheses without and with small amounts of expander lead to ordered cylindrical pores. Increasing the expander to P123 molar ratio towards 36 results in a loss of the regular alignment of the pore openings (Table 1) without indication of spherical (foam-like) pores. As the expander amount increases the maxima of the pore size distribution curves shift progressively from 7.5 nm for SBA-15 (Fig. 3b and d, black curve) to ~19 and ~17 nm for TMB-36 and LIM-36 (Fig. 3b and d, green curve). Further increase in the expander amount does not result in further increase of the pore sizes, indicating that the maximum expansion of the pores has been achieved at a ratio of 36 for both the expanders. Textural data for all the samples are listed in Table 1. These results clearly demonstrate the pore expanding capabilities of limonene and show that it is very similar to TMB.

In addition to the pore size, the expander amount also has a major influence on the pore morphology and arrangement which was visualised through transmission electron microscopy (TEM) analysis (Fig. 4). In the sample synthesised without the expander (Fig. 4a) we observe hexagonally arranged cylindrical pores which are characteristic of SBA-15.[12] The addition of small amounts of expanders TMB and limonene, respectively, widens the pore space and still results in long channel-like pores that run parallel along the entire particle (Fig. 4b and e). In contrast to the reference sample (SBA-15), these channels twist and turn at different angles, which correlates with the changed morphology of the porous particles (Fig. 5b and i). Further increase of the amount of both expanders leads to progressive loss of the ordered arrangement of the pores. In the case of TMB this structural loss is already pronounced for an expander/P123 molar ratio of 16 (Fig. 4c) and in the case of limonene at an expander/P123 ratio of 36 (Fig. 4g). Accordingly, at an expander/P123 ratio of 36, a similar pore morphology is obtained for both expander molecules with no further increase of pore size, pore volume and surface area as seen from the nitrogen physisorption results (Table 1).

Scanning electron microscopy (SEM) was used to compare the influence of both expander molecules on the particle
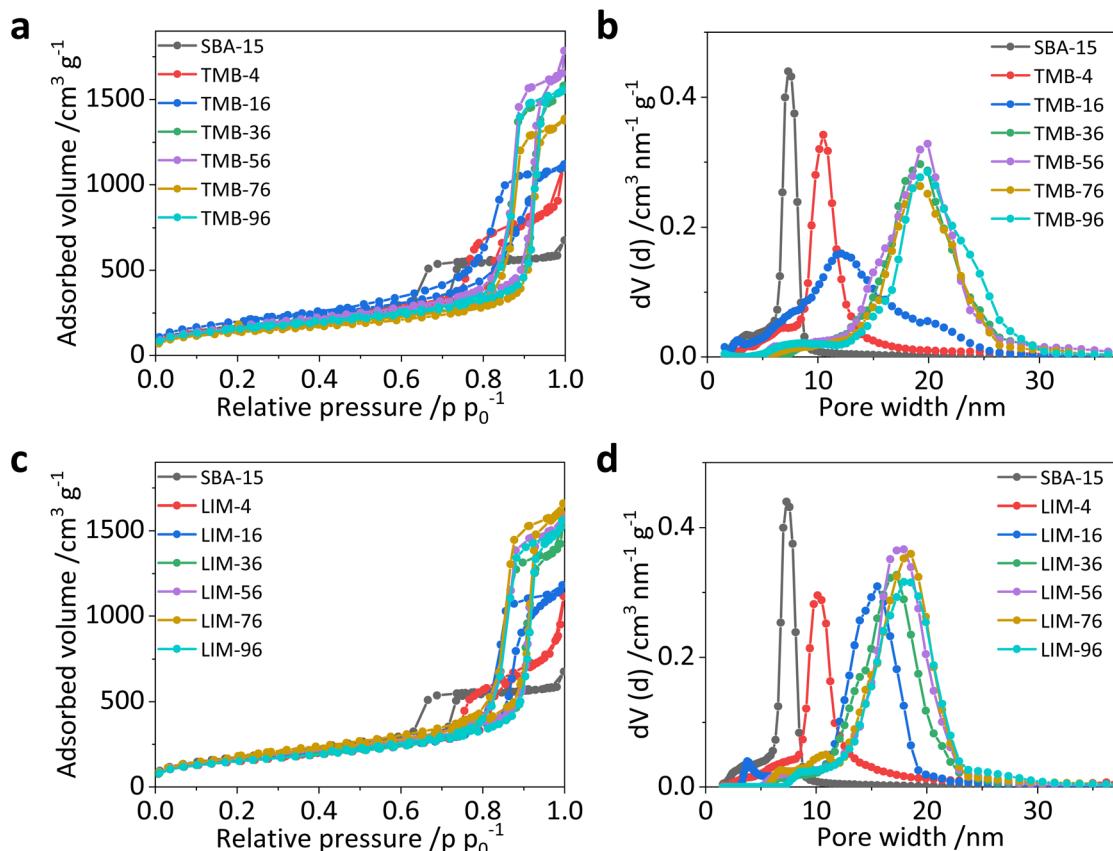
Fig. 3 N$_2$ physisorption data for varying amounts of TMB (top row) and limonene (LIM, bottom row) expander. The isotherms for samples synthesised using (a) TMB and (c) limonene are all of type IVa. The pore size distributions in (b) and (d) show a gradual increase in pore size with increasing expander to P123 molar ratio.

Table 1 Textural data for samples obtained with different amounts of the expanders, limonene (LIM) and TMB, respectively

Sample	Pore size[a] (nm)	Specific surface area (m^2 g^{-1})	Total pore volume (cm^3 g^{-1})
SBA-15	7.5	625	1.0
TMB-4	10.5	618	1.4
TMB-16	12.2	666	1.7
TMB-36	19.3	603	2.4
TMB-56	20.0	594	2.6
TMB-76	19.3	482	2.1
TMB-96	19.9	532	2.4
LIM-4	10.2	528	1.5
LIM-16	15.5	542	1.7
LIM-36	17.5	609	2.4
LIM-56	18.0	570	2.4
LIM-76	18.5	590	2.5
LIM-76	18.5	590	2.5

[a] Mode pore diameter determined from the maximum of the pore size distribution curve.

morphology (Fig. 5, S3†). For the sample with no expander, we see a faceted morphology that has been previously observed for SBA-15 materials.[39] With the addition of small expander amounts (TMB-4 and LIM-4), the particles transform into long agglomerated strands (Fig. 5b and h). As observed in the TEM images, these strands contain long twisted channels running parallel through the entire particle (Fig. 4b and e). When the expander amount is further increased (expander/P123 ratios of and above 16), the particles show a spherical agglomerated morphology (Fig. 5c–g and i–m) which is similar for both, TMB and limonene. Here, the expanded pore entrances are already visible at the particle surface.

The pore structure of the samples was further examined using the small angle X-ray scattering (SAXS) technique (Fig. 6). The 1D SAXS profile of the reference sample (SBA-15) shows several strong scattering peaks (Fig. 6, blue line) whose positions have a relative ratio of $1 : \sqrt{3} : \sqrt{4} : \sqrt{7}$. This corresponds to a well-ordered hexagonally close-packed (HCP) superstructure,[40] which is expected for SBA-15.[41] The extracted lattice parameter is 11.1 nm, representing the pore centre–centre distance of HCP cylindrical pores in the sample. Together with the TEM-based pore wall thickness of 3.3 nm the calculated pore diameter of 7.8 nm agrees well with the results from nitrogen physisorption (7.5 nm). For the sample with a low ratio of expander/P123 (LIM-4), the HCP pore structure persists, however the lattice parameter increases to 12.7 nm. When the amount of limonene is further increased (LIM-16), a transition from HCP to a less ordered structure at a repeating distance of 13.3 nm is observed
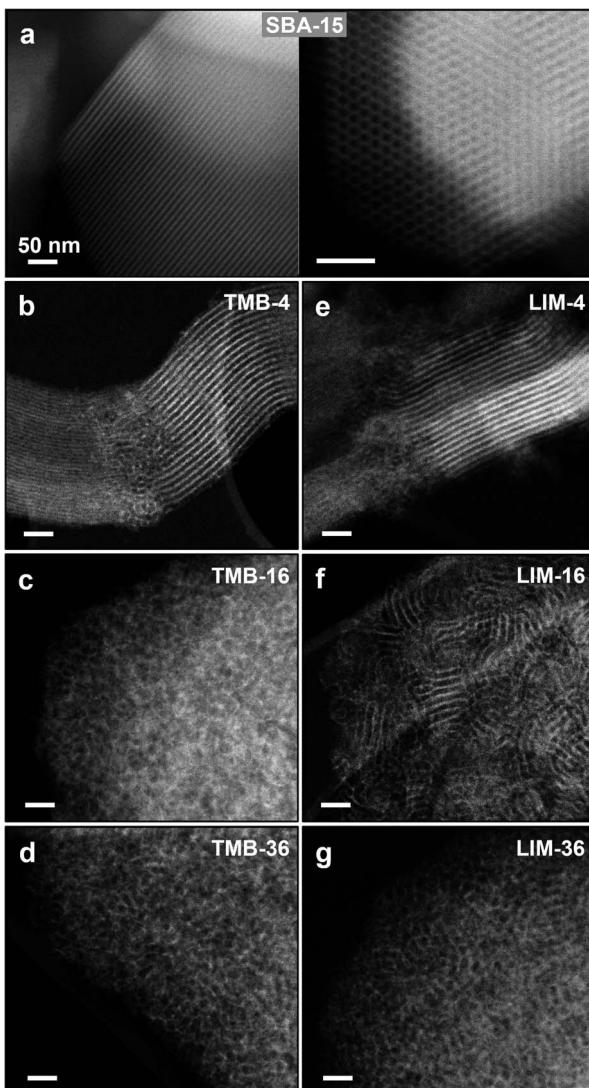
Fig. 4 TEM images for mesoporous silica synthesised with increasing expander/P123 molar ratios from 4 up to 36 for both TMB (left column) and limonene (right column). As a reference the SBA-15 sample synthesised in the absence of expander molecules is depicted in the upper image (a) showing the cylindrical pores in side-view (left) and viewed along the pore channels (right). The scale bar for all images is 50 nm.

with scattering peaks at ratios of $1:2:3$. For further increase in expander amount (LIM-36, LIM-56, LIM-76), the scattering profiles show peak broadening which suggests that the pore arrangement becomes less ordered with a periodic distance of 18.4–19.6 nm. Similar results are observed for the TMB samples. For the sample with a low amount of expander (TMB-4), the scattering peaks have an intermediate peak position ratio, which corresponds to a distorted HCP or body centred rectangular superlattice with a pore-to-pore distance of 12.9 nm. For higher TMB amounts, the system goes through a systematic structural transition with an increase of the pore-to-pore distance to 22.6 nm. However, the overall broader scattering peaks for these samples indicate relatively less ordered structures compared to the limonene samples. The scattering peaks
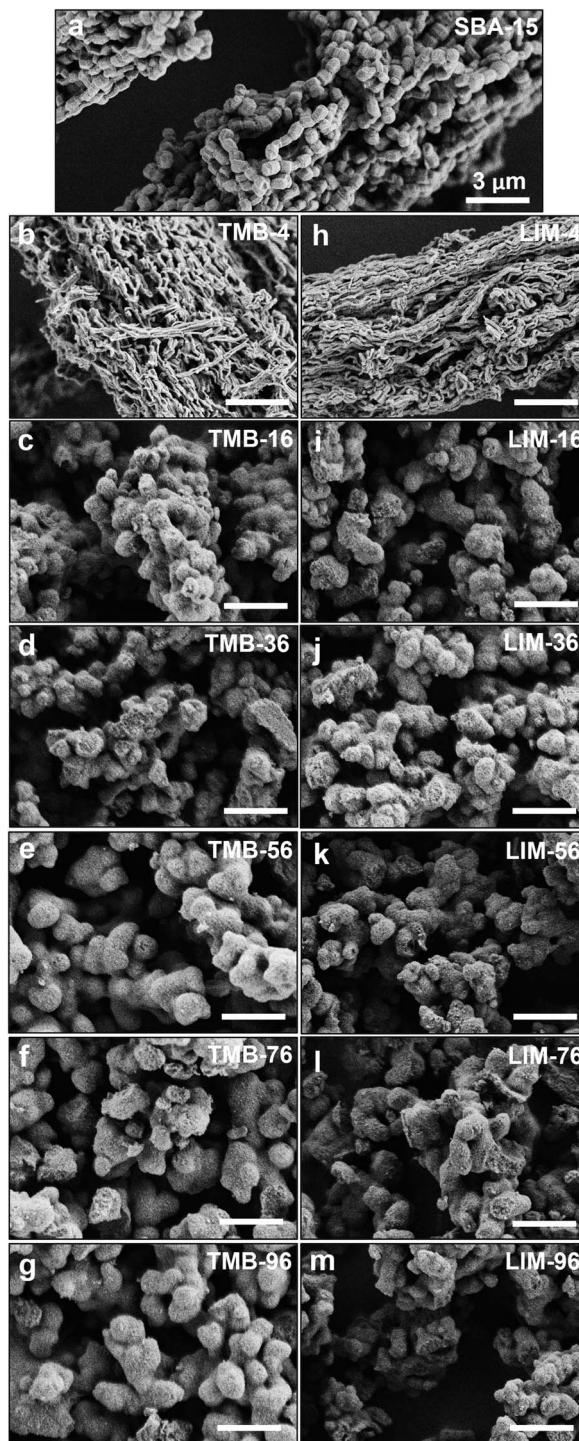

Fig. 5 SEM images of SBA-15 (a) and pore expanded micellar templated silica obtained with increasing amounts of expander TMB (left column) and limonene (right column). The scale bar is 3 μm for all images.

for the expander-rich samples (TMB-36, TMB-56 and TMB-76) have a positional ratio of $1:\sqrt{2}:\sqrt{4}$, which implies a body centred cubic (BCC) superlattice structure. Interestingly, the patterns remain unchanged with further increase of expander amount, indicating that the pore expansion and structural
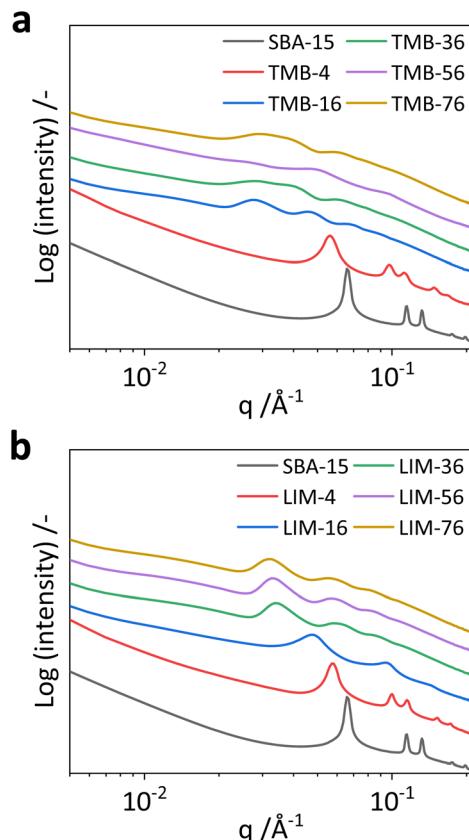
Fig. 6 Small angle X-ray scattering (SAXS) patterns for mesoporous materials with various amounts of pore expanders. Sharper reflexes for SBA-15 samples shift to the left and become broader with increasing amounts of expander for both, (a) TMB and (b) limonene.

transformation is complete. Overall, the SAXS data show that both expander molecules, TMB and limonene, have similar effects on the mesopore structure formation, though the use of limonene results in a slightly more ordered pore arrangement compared to TMB under the synthesis conditions used in our experiments.

Life cycle assessment

A life cycle assessment (LCA) was performed to identify which of the two expander molecules is greener: petrochemical-based 1,3,5-trimethyl benzene (TMB, mesitylene) or limonene produced as a by-product of the orange juice production. The LCA was conducted in four steps according to DIN 14040/14044: goal and scope definition, inventory analysis, impact assessment and interpretation.[42,43]

Goal and scope definition. In the first part of this contribution, it was shown that a similar mole fraction of bio-based expander molecule limonene is required to substitute TMB in order to obtain a pore-expanded silica material with comparable properties. On this basis the functional unit for the LCA was chosen to be the production of 1 t of expander molecule for both, TMB and limonene. The cut-off-criterion was set at in-/outputs less than 1.5%.

The system boundary is cradle-to-gate, *i.e.*, from raw materials sourcing until the produced expander molecule (Fig. 7). However, for the production of limonene two different allocation scenarios were chosen to deal with the 'waste' status of the orange peels.[44] In scenario (a) the orange peels are considered left-over waste from orange juice production as it is currently the case. Therefore, the impacts of orange tree cultivation, harvesting and orange fruit processing are solely allocated to the orange juice production. In scenario (b) we assume the (bio-based economy) case that limonene (and other organic molecules) production from orange peels establishes as an economic factor for orange fruit processing. In this case the orange trees are not only harvested for orange juice production but also for the production of limonene and other valuable organic products like molasses, which justifies that at least 5% (equal to the weight portion of limonene among the other valuable organic components in the organic fraction of orange peels of oranges) of the environmental impacts for cultivation, harvesting and orange fruit processing are allocated to the orange peel production from which limonene is extracted.

The greenness evaluation is based on the calculation of the midpoint indicators: fossil resource scarcity (FRS), freshwater eutrophication potential (FWE), global warming potential (GWP), human carcinogenic toxicity potential (HTP), land use potential, terrestrial acidification potential (TAP) and water consumption (depletion) potential (WDP).

Inventory analysis. In Fig. 7 the process steps for the production of TMB and limonene from their respective raw materials as well as the system boundaries for the mass and energy balance are visualised.

TMB is produced *via* self-condensation of acetone.[45] The production process was not available in the ecoinvent database. Therefore, we simulated this process using the AspenPlus NRTL model to estimate the respective energy input based on the literature data[45] for 80% conversion, 70% selectivity to TMB, a reaction temperature of 350 °C, pressure of 1 bar and a niobium on silica catalyst (2 wt% of the reaction mixture), which has to be regenerated after 150 h time on stream through calcination at 550 °C for 18 h.[45] In addition to TMB, by-products such as mesitylene oxide, isobutene, acetic acid, C10 and C12 cyclic hydrocarbons are produced, which are valuable products. Therefore, the impacts of the self-condensation process have been allocated also to these by-products according to the selectivity (20% by-products).

Acetone is industrially obtained as a by-product of the cumene process (Hock process), where benzene and propene react to form cumene, which is then oxidised with air to cumene hydroperoxide, which is finally split into phenol and acetone.[46,47] Together with each kg of phenol, 0.63 kg of acetone is produced.[48] Data about this process are already available in the ecoinvent database. The energy and mass inputs, and the respective environmental impacts of the cumene process are partially allocated to phenol according to its produced fraction. Therefore, phenol is not included in the calculation of the environmental impacts of acetone production and also not included in the product system. Propene stems from crude oil
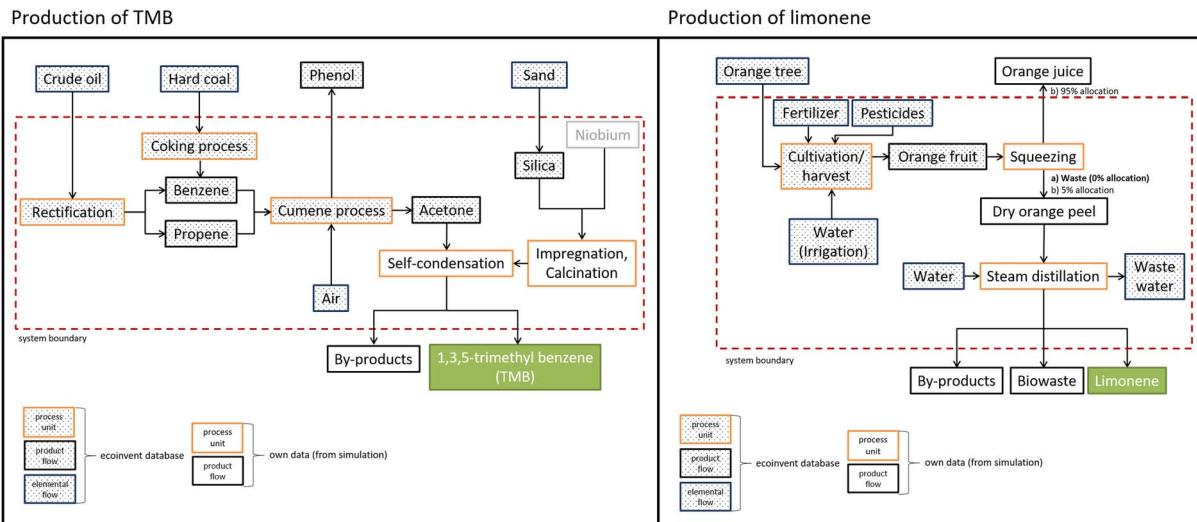
Fig. 7 Process flow charts and LCA system boundaries for the production of TMB and limonene. For limonene two allocation scenarios are considered: (a) the orange peels are left-over waste from orange juice production without allocation of the environmental impacts of the pre-processes to the orange peels, (b) the orange peels are considered a resource and accordingly, the orange trees are not only harvested for orange juice production but also for the production of limonene and molasses, therefore 5% of the environmental impacts of cultivation, harvesting and orange fruit processing are allocated to the orange peel production from which limonene is extracted.

processing, benzene from crude oil and coal, which was also available in the ecoinvent database.

For limonene we assessed the industrial production process from orange peels, which is currently (scenario (a)) a waste product of the orange juice production.[49,50] Squeezing of oranges yields around 60 wt% juice. The remaining 40 wt% is wet orange/citrus processing waste, which consists mainly of orange peel including the segment membranes.[51] The major components of this waste are 80 wt% water, 6 wt% soluble sugars, 5 wt% cellulose and hemicellulose, 4 wt% pectin and 0.8 wt% limonene.[50,52] To isolate the limonene, steam distillation is the industrially applied process which recovers around 65 wt% of the limonene in the orange peel waste with a purity of 95%.[49,53] From these data it was calculated that around 192 t of orange peel is needed to produce 1 t limonene (see Fig. 8). The organic residues remaining as the bottom product after the steam distillation contain other valuable products like molasses which can be further processed to, *e.g.*, compounds for perfumes[49,50] and bioethanol[53] for which we assume a yield of 20 t together with each tonne of limonene, which led to the 5% allocation for limonene in scenario b. The 148 t of waste water per t limonene resulting from the steam distillation might be treated in conventional activated sludge facilities (volume of 10^9 l/a), where limonene residues are biodegraded in the aeration basin.[54] The contribution of this treatment to the life cycle impacts of limonene is very small (below 1%) and therefore not further considered.

Data for the harvesting of oranges in Spain were available in the ecoinvent database. Data for the production of orange juice yielding orange peels as a by-product were obtained from the literature.[43,49,50] Only the data for steam distillation of the orange peels for the production of limonene had to be simulated to obtain the energy requirements based on process

parameters given in the literature.[49,50,55] The reaction parameters and the process flow sheets of both simulated processes (TMB production *via* acetone self-condensation; limonene production *via* steam distillation of orange peels) can be found in the ESI in Tables S2, S3 and Fig. S4, S5.†

As can be seen from the inventory data in Fig. 8, the cradle-to-gate production of 1 t TMB (*via* acetone self-condensation starting from crude oil and hard coal as visualised in Fig. 7)
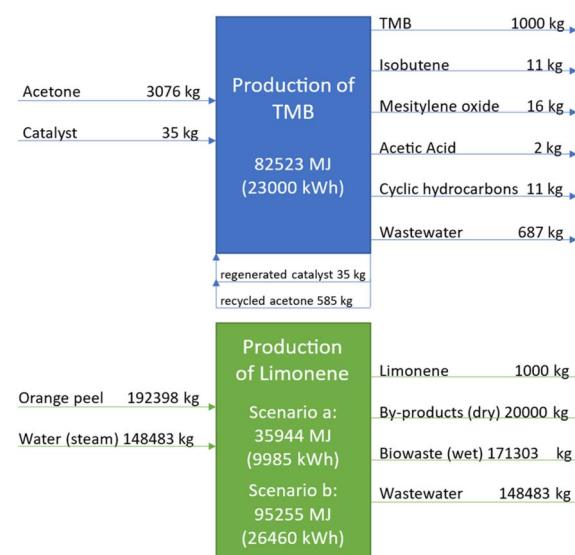

Fig. 8 Life cycle inventory: mass inputs and outputs and total allocated energy consumption for the cradle-to-gate production of TMB *via* self-condensation of acetone and production of limonene *via* steam distillation of orange peels, which are treated as waste (scenario a) or chemical resource with 5% of the impacts for orange tree harvesting and fruit processing allocated to the orange peels (scenario b).

requires a total energy of about 82 523 MJ. Table 2 details the respective energy contributions of the different process units which are allocated to the production chain of TMB within the LCA system boundaries. From there it can be seen that the largest contributors to the energy consumption of TMB production are the acetone self-condensation process (25 163 MJ = 30% of the total energy demand) and the cumene process (27 071 MJ + 27 093 MJ = 66% of the total energy demand).

The total energy demand to produce 1 t limonene depends strongly on the allocation of the energy requirements of the pre-processes (orange tree harvesting up to the generation of the orange peels). The steam distillation process for the production of 1 t limonene requires almost 192 t orange peels and is therefore associated with an enormous amount of water steam which has to be generated for the extractive distillation, which consumes 35 944 MJ energy. If the pre-processes for the orange peels are not allocated to limonene (waste scenario a) then the cradle-to-gate production of 1 t limonene counts only the energy for the steam distillation of the orange peels, *i.e.*, 35 944 MJ, which is less than half of the energy demand for TMB production. If the orange peel pre-processes are allocated with 5% to limonene (value product scenario b) then 5% of the energy consumption of orange tree plantation and harvesting, *i.e.*, 38 876 MJ, and 5% of the energy consumption of the orange fruit squeezing process, *i.e.*, 20 387 MJ, have to be added to the steam distillation demand, leading to a total cradle-to-gate energy requirement of 95 255 MJ, which is 15% more than the energy required for TMB production.

Furthermore, Fig. 8 details the output streams of the production of TMB and limonene, respectively. Acetone reacts *via* self-condensation to form TMB. The unconverted acetone (25%) is recycled back into the process. Around 5 wt% of the output is by-products like cyclic hydrocarbons, acetic acid, mesityl oxide and isobutene. Since these are value products, 5% of the process impacts is allocated to them and not to TMB.

Impact assessment and interpretation. In general, if a chemical is called "greener" it should have less environmental impacts compared to its conventional counterpart. To assess such potential environmental impacts quantitatively, several impact categories have been defined with their respective indicators which are calculated from the outputs of the mass and energy balances obtained in the inventory analysis of the life cycle assessment.

Accordingly in our case, an expander molecule and the MTS synthesis using this expander molecule would be greener if its potential impact on, *e.g.*, fossil resource depletion, global warming, water pollution and human health is less.

As can be seen in the left spider chart in Fig. 9, limonene (green curve) has much lower environmental impacts than TMB if it is produced from orange peel waste. The significant contributions of limonene production to freshwater eutrophication, global warming, and human carcinogenic toxicity stem solely from use of the conventional energy mix (containing 50% coal, gas, oil and radioactive sources) because they disappear completely if the energy mix is changed to 100% renewable (Fig. 9, top right).

In a future bioeconomy, where limonene might become a more important chemical whose demand exceeds the generation of orange (citrus) peel waste and might lead to the plantation and harvesting of orange fruit not only for juice but also for limonene production, the allocation scenario b (5% allocation of the pre-process impacts to limonene production) will be of relevance. In this case, using the conventional energy mix, limonene production shows worse effects in almost all impact categories compared to TMB, except for fossil resource scarcity and global warming potential. Looking at the process contributions for limonene in Fig. 9 (bottom right; absolute values are given in Table S4†), the reason for this worse effect is the high amount of energy required for the steam distillation step. Here, we assumed the current German electricity mix, of which only 50% is renewable energy.[56] Also the current energy sources used in Spain for growing and processing oranges are mostly oil and coal power-based, which strongly influence environmental impacts such as freshwater eutrophication potential, global warming potential and human carcinogenic toxicity.[56] Typical lorry transport of dry orange peel (192 t per t of limonene) within Europe, *e.g.*, from Spain to Germany, also contributes to

Table 2 Allocated energy demands of the process units for the production of 1 t TMB and limonene

Process unit	Product	Allocated energy demand/MJ
Production of TMB		
Coking process	Benzene	2455
Rectification	Benzene	44
	Propene	678
Cumene process	Cumene (1st stage)	27 071
	Acetone (2nd stage)	27 093
Self-condensation	TMB	25 163
Catalyst preparation and regeneration	Nb@ZSM-5	11
Production of limonene		
Orange plantation	Orange fruit	38 876
Squeezing	Orange peel	20 387
Steam distillation	Limonene	35 944
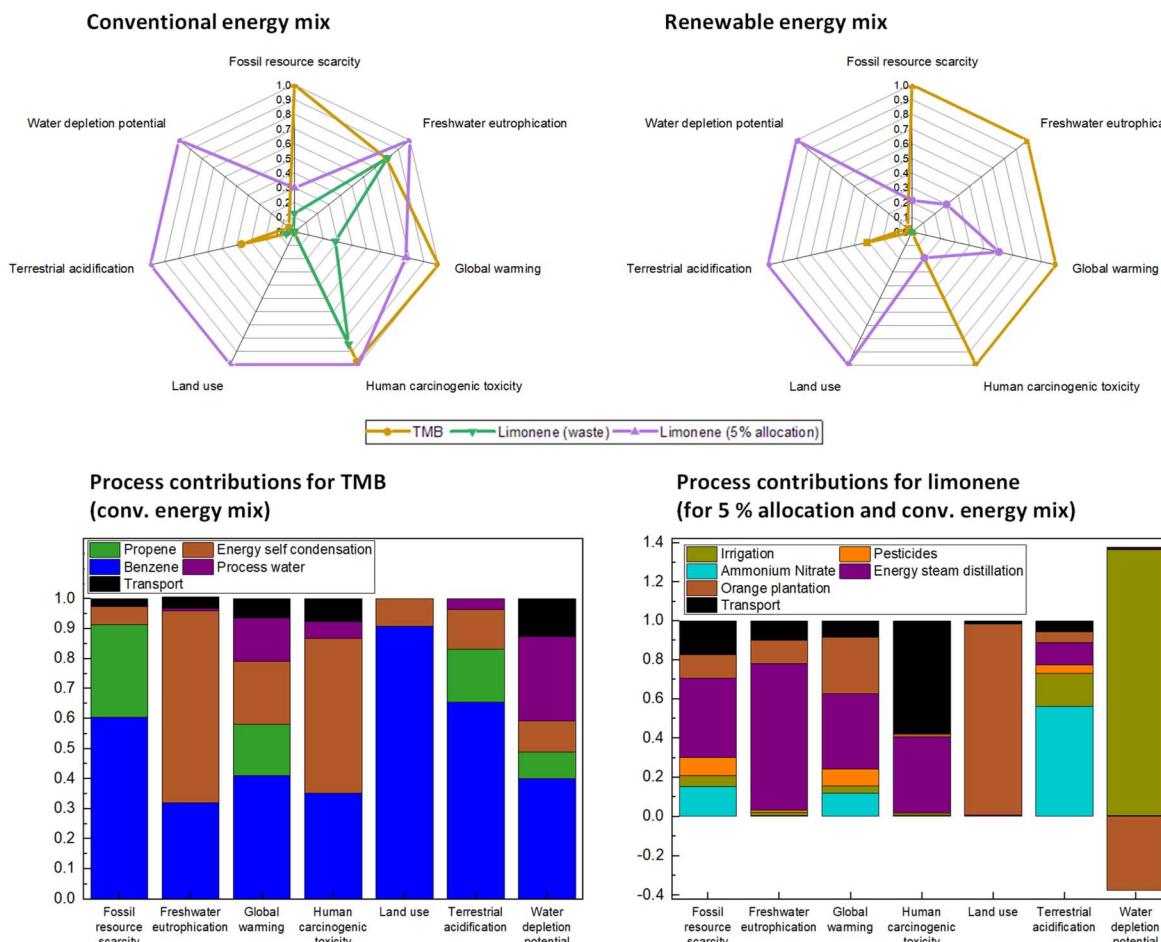
Fig. 9 Spider charts comparing the allocated potential environmental impacts of the production of the two expander molecules using the conventional energy mix (top left) and using 100% renewable energy for the gate-to-gate production part (top right); bottom: detailed bar charts for the relative process contributions to the environmental impacts for the cradle-to-gate production using the conventional energy mix for TMB (left) and limonene (right, scenario b with 5% allocation). Absolute values for the environmental impact indicators are summarised in Table S4.†

the life cycle impacts of limonene production (Fig. 9, bottom right), which is around 17% for fossil depletion and even 58% for human toxicity potential due to the exhaust emissions from fuel. These impacts could be largely reduced if trains instead of lorries would be used or if the orange peel would be extracted directly at the place of citrus peel generation. The high land use and water consumption of limonene production is caused by the cultivation of the orange tree plantations. Since the content of limonene in orange (citrus) peels is quite small (see Fig. 8), a large number of citrus trees have to be cultivated to yield 1 t of limonene.

In the production of TMB, the intermediate benzene production (67% from crude oil processing, 33% from coal coking) has a strong influence on all environmental impacts (Fig. 9, bottom left, absolute values are given in Table S5†). Propene, on the other hand, which is mainly produced *via* steam cracking of longer-chain alkanes (C5–C10) or naphtha, has a much lower influence on the potentials compared to benzene production. The contributions of transport to the TMB impacts are due to the offshore pipeline delivery of crude oil for

propene production, which we assumed from Russia to Germany and which impacts especially the water depletion potential. Furthermore, for benzene production also hard coal is needed, for which we assumed import from Russia *via* train and which is the main transport contribution to human toxicity potential.

To show how a (future) fossil-free energy mix of 100% renewable energy sources (composed of 95% hydro power, 2% wind power, 3% biomass) would influence the environmental impacts of TMB and limonene production, we added the spider chart for the scenario '100% renewable energy' in Fig. 9 (top right). The potential impacts of limonene production (scenario with 5% allocation) on fossil resource scarcity, freshwater eutrophication, global warming, and human carcinogenic toxicity are significantly reduced if the energy demand (which is especially high for the steam distillation step) is covered by this 100% renewable energy mix. We used the hydro power-rich energy mix because it is the only renewable energy mix currently available in the ecoinvent database. However, the literature on life cycle impacts of different energy sources shows

that the main impact differences are between fossil-based and renewable sources. The type of renewable energy source does not have a significant contribution.[57,58]

Independent of the energy mix, in scenario (b) the potential impacts of limonene production on land use, acidification potential (due to fertiliser use) as well as water consumption (for irrigation) are always higher compared to TMB. This stems primarily from the orange tree plantation. In general, it is typical for chemicals from renewable sources that their production impacts these three impact categories much more compared to fossil-based chemicals where no trees or plants have to be grown and it will be the task of future (sustainable) farming systems to reduce these impacts as much as possible, especially if an increased amount of chemicals is to be produced in this way.

For the current scenario (a), where the orange peels are still a waste product of the food industry, the environmental impacts of limonene production using 100% renewable energy are remarkably low and close to neutral. Accordingly, the LCA-based claim of limonene being a greener expander molecule than TMB (and many other fossil-based molecules) for the preparation of porous materials is very valid at the moment but bound to the precondition that it is produced from citrus fruit waste and not from citrus fruit which is purposefully grown for the production of limonene. Otherwise, limonene will only be greener than TMB in terms of fossil resource scarcity potential, global warming potential and (if 100% renewable non-biogenic energy sources are used for its production) also human carcinogenic toxicity and freshwater eutrophication potential.

If green metrics, namely process mass intensity (PMI) and environmental factor (E-factor), are used instead of LCA then TMB production occurs much greener than limonene production. The values are calculated according to eqn (1) and (2) in the experimental section, based on the process input and waste output streams given in Fig. 8 and summarised in Table 3. The PMI values indicate that the gas phase conversion of acetone to TMB requires much less input compared to limonene, which is obtained *via* steam distillation of a large quantity of dried orange peel. If the water used for the steam distillation is also considered (PMI$_{RRC+Solv}$) then the PMI for limonene is even higher, *i.e.*, worse. Also, the E-factor, which quantifies the waste produced per amount of target chemical, is much higher for limonene than TMB, which is due to the high amount of remaining biowaste and wastewater from steam distillation. However, the comparison is probably quite unfair because in contrast to TMB, the input for limonene production is already a waste product (waste orange peel). It also shows that the reuse of the water after steam distillation would make the process greener. In general, the LCA results indicate that the main contributions to environmental impacts for

Table 4 Names and molar ratios of chemicals used for all the synthesized samples

Sample	P123	Expander	TEOS	HCl	H$_2$O	NH$_4$F
SBA-15	1	0	59	350	9200	2
TMB-4	1	4	59	350	9200	2
TMB-16	1	16	59	350	9200	2
TMB-36	1	36	59	350	9200	2
TMB-56	1	56	59	350	9200	2
TMB-76	1	76	59	350	9200	2
TMB-96	1	96	59	350	9200	2
LIM-4	1	4	59	350	9200	2
LIM-16	1	16	59	350	9200	2
LIM-36	1	36	59	350	9200	2
LIM-56	1	56	59	350	9200	2
LIM-76	1	76	59	350	9200	2
LIM-96	1	96	59	350	9200	2

the chemical production are caused by high energy consumption of the different production steps (also in pre-processes), which is not considered in PMI and E-factor, thus giving an incomplete (only gate-to-gate) picture. Besides, the cultivation and irrigation of oranges and other citrus fruits has a high impact on terrestrial acidification. With better irrigation systems and a change to ecological/sustainable agriculture instead of monocultures, which avoid the consumption of artificial fertilisers and pesticides and enable an intensive irrigation, the environmental impacts of limonene-based applications will be further reduced. For the production of micellar templated silica materials, a shortage of citrus peel waste-based limonene is currently not expected. Even if limonene would replace all TMB in its applications (for which the world production is 10 000 t/a[59] and only a minor fraction is used as the expander molecule for MTS materials) just 3% of the global waste-based limonene production (which is 368 000 t/a obtained from 115 million t/a citrus fruit[55]) would be required.

However, if in future the demand for limonene exceeds the generated amount of citrus peel waste, then also other sources for limonene production (*e.g.*, turpentine oil) and the use of alternative renewable molecules have to be considered on the basis of further comparative life cycle assessments to avoid over-burdening of the natural environment with process-related impacts.[60] Furthermore, limonene also poses some chemical hazards (*e.g.*, very toxic to aquatic life, skin irritant and may be fatal if swallowed or inhaled). Therefore, future research should also focus on identifying other suitable bio-based expander molecules with lower toxicity and ideally lower life cycle impacts to make the synthesis of micellar templated silica materials even greener.

Conclusion

Pore-expanded micellar templated silica materials were synthesised using limonene as a renewable alternative for the conventionally applied pore expander trimethylbenzene (TMB) and the effect of both expander molecules on the resulting material properties was compared. Nitrogen physisorption analysis showed that the same amount of limonene is needed to successfully expand the pore size from 7.5 nm (without the

Table 3 E-factors and PMI for the production of limonene and 1,3,5-trimethyl benzene (TMB); PMI$_{RRC}$ does not include the solvent

	PMI$_{RRC}$	PMI$_{RRC+Solv}$	E-factor
Limonene	192	341	320
TMB	3.1	3.1	0.7

expander) up to the largest possible extent of 17–19 nm (19–20 nm for TMB). TEM and SEM analyses indicated similar pore and particle morphologies obtained with limonene and TMB, respectively. Together with SAXS analysis, a slight difference between the action of TMB and limonene was found in the maintenance of an ordered pore structure up to an expander/P123 molar ratio of 16 for limonene, while with TMB the structural loss was already more pronounced at this expander amount. However, at a ratio of 36 the transformation towards a disordered pore structure with the maximum pore diameter was complete for both expanders, which demonstrates that limonene is a versatile substitute for fossil-based TMB because it can fully overtake its function as a pore expander.

A cradle-to-gate life cycle assessment (LCA) for both expander molecules proved that limonene is indeed a very green substitute for TMB if it is produced from citrus/orange peel waste, especially if a 100% renewable energy mix is used, which is generally very desirable for a sustainable development (UN SDGs 7 and 13).

With our study we hope to stimulate further exploration of renewable organic molecules as well as respective recovery and recycling procedures for greener syntheses of porous materials and their application, which would be a valid contribution to a more sustainable material basis for our society (UN SDG 12).

Experimental section

Materials

Hydrochloric acid (HCl, 37%, VWR), Pluronic P123 (P123, 5800 g mol^{-1}, Sigma-Aldrich), 1,3,5-trimethylbenzene (TMB, ≥98.5%, Thermo Scientific), limonene (≥95%, D and L type mixture, Sigma-Aldrich), ammonium fluoride (NH$_4$F, 98%, Sigma-Aldrich), tetraethyl-orthosilicate (TEOS, ≥99%, GPR RECTAPUR®, VWR) and sodium hydroxide (NaOH, ≥98%, in pellets, VWR) were all used as received. De-ionised water was used for all synthesis and cleaning procedures. All reaction vessels were cleaned using 5 wt% aqueous NaOH solution, before use. Commercial silica gel "grade 62" was purchased from Sigma Aldrich.

Synthesis of SBA-15 and pore-expanded micellar templated silica

In a typical procedure, 20.55 g of water and 4.93 g of hydrochloric acid were mixed and 0.83 g of P123 was added to it at room temperature. The solution was stirred at 500 rpm in a 60 mL polypropylene (PP) bottle with a circular cross-section of 4 cm containing an elliptical magnetic stirring bar (32 mm × 15 mm). The reaction vessel was kept closed with a screw cap and was only opened when adding further reactants. Then the necessary amount of micelle expander (0.07 g for sample TMB-4, 0.3 g for TMB-16, 0.6 g for TMB-36, 1 g for TMB-56, 1.3 g for TMB-76, 1.3 g for TMB-96, 0.08 g for LIM-4, 0.3 g for LIM-16, 0.7 g for LIM-36, 1.1 g for LIM-56, 1.5 g for LIM-76, 1.9 g for LIM-96) and 0.01 g of NH$_4$F were added. After stirring for 1 h, 1.75 g of TEOS was added. The molar ratios used for all the samples are listed in Table 4. After 1 h of further stirring, the

reaction vessel (PP bottle) was placed in a circulating oven at 40 °C for 20 h. Afterwards, the solution was transferred to a 45 mL polytetrafluoroethylene (PTFE) lined autoclave (Parr). The autoclave was then placed in the circulating oven at 100 °C for 24 h. Afterwards, the autoclave was allowed to cool down. Its contents were then centrifuged (6500 rpm for 5 min) and the sediment was washed 2 times with ethanol and one time with water. The obtained material was then dried at 75 °C overnight. The dried sample was then crushed in a mortar and transferred to a heat-resistant ceramic crucible. The crucible was placed inside a calcination furnace and heated to 550 °C with a ramp of 2 °C min^{-1}, under an airflow of 50 L h^{-1}, for 6 h to remove any organic residues. After calcination, the sample was again crushed with a mortar and transferred to a sample container.

Nitrogen physisorption

All the samples were degassed prior to measurements using a vacuum degasser (MasterPrep Degasser, Quantachrome Instruments) at 250 °C for 12 hours. The nitrogen physisorption measurements were conducted using a Quadrasorb (Quantachrome Instruments) at 77 K. The specific surface area was calculated using the Brunauer, Emmett and Teller (BET) method in the relative pressure range from 0.05 to 0.36 and the micropore volume was determined using the t-plot in the range from 0.3 to 0.5 p/p$_0$. The pore size distributions were calculated using the non-linear density functional theory (NLDFT) model for cylindrical pores from the adsorption and desorption branches of the isotherms.

Scanning electron microscopy (SEM)

The SEM analysis was conducted via a GeminiSEM 500 (Zeiss) using a secondary electron detector. The measurements were performed at 1 kV voltage with an aperture size of 15 µm.

Transmission electron microscopy (TEM)

The TEM analysis was carried out in high-angle annular dark-field scanning transmission electron microscopy (HAADF-STEM) mode using a Titan Themis³ 300 transmission electron microscope (Thermo Fisher Scientific). The images were acquired at 300 kV.

Small angle X-ray scattering (SAXS)

SAXS measurements were carried out with an in-house SAXS setup (VAXSTER; Versatile X-ray Scattering Instrument Erlangen) in transmission geometry.[61,62] It uses a 250 W liquid gallium jet X-ray source (Excillum) providing an X-ray wavelength of 1.34 Å. The powder samples were filled in 1 mm glass capillaries and placed at the sample position inside the evacuated (~10^{-3} mbar) detector tube. The X-ray beam was monochromatised and focussed through a 2.5 m collimation line with 3 double slit systems (two of which were equipped with single crystal scatterless Si blades) to a beam cross-section of ~0.36 × 0.36 mm² at the sample position by a 15 cm Montel optics (Incoatec). A Dectris Pilatus3 300k detector was used to record the SAXS images at a sample-to-detector distance of 1.6 m. The

X-ray path was fully evacuated, and each measurement was collected for 1 hour for sufficient statistics. The collected 2D isotropic SAXS patterns were azimuthally averaged and the resulting 1D scattering profiles were plotted and analysed.

Life cycle assessment (LCA)

In this study, a comparative assessment of the greenness (ecological impacts) of the two expander molecules, namely the petrochemical-based trimethylbenzene (TMB) and the bio-based limonene, was undertaken in the context of an LCA. The LCA was conducted according to DIN EN ISO 14040/44 (ref. 42) with goal and scope definition, inventory analysis, impact assessment and interpretation. For data management, the LCA software openLCA (version 10.1.3) and the database ecoinvent 3.7.1 were used. Calculation method for the midpoint categories was ReCiPe 2016 midpoint (H).[63] Energy input data which were not available in the ecoinvent database were simulated using the programme Aspen (version 10). The parameters used for these simulations are detailed in Table S2 in the ESI.†

Green metrics

The PMI is calculated from the amount of reagents, reactants and catalyst (PMI_{RRC}) and solvent (PMI_{Solv}) relative to the amount of isolated product:[64,65]

$$PMI = \frac{mass_{reactants} + mass_{reagents} + mass_{catalyst} + (mass_{solvent})}{mass\ of\ isolated\ product} \quad (1)$$

The E factor is calculated from the amount of waste in relation to the amount of mass of the product:[66]

$$E\ factor = \frac{total\ mass\ of\ waste}{mass\ of\ product} \quad (2)$$

Author contributions

U. S. designed and realised the experiments, performed the synthesis, characterisation, analysis, and interpretation. D. L. performed the synthesis. U. S. and A. I. conceptualised and supervised all the research work and wrote the original manuscript. K. S., A. G. and A. I. performed the LCA. E. M. and S. M. performed SAXS characterisation, analysis, and interpretation. C. S. and M. T. performed interpretation of textural characterisation. T. Y. and B. A. Z. performed TEM characterisation. E. S., N. V., T. U., M. T., and A. I. acquired the funding. All authors reviewed and edited the final manuscript.

Conflicts of interest

There are no conflicts of interest to declare.

Acknowledgements

References

1 H. C. Erythropel, J. B. Zimmerman, T. M. de Winter, L. Petitjean, F. Melnikov, C. H. Lam, A. W. Lounsbury, K. E. Mellor, N. Z. Janković, Q. Tu, L. N. Pincus, M. M. Falinski, W. Shi, P. Coish, D. L. Plata and P. T. Anastas, *Green Chem.*, 2018, **20**, 1929–1961.

2 J. B. Zimmerman, P. T. Anastas, H. C. Erythropel and W. Leitner, *Science*, 2020, **367**, 397–400.

3 J. Florek, R. Guillet-Nicolas and F. Kleitz, in *For Energy, Sustainable Development and Biomedical Sciences*, ed. M. Leclerc and R. Gauvin, De Gruyter, 2014, pp. 61–100.

4 X. Yu and C. T. Williams, *Catal. Sci. Technol.*, 2022, **12**, 5765–5794.

5 C. Bonzom, L. Schild, H. Gustafsson and L. Olsson, *BMC Biochem.*, 2018, **19**, 1.

6 I. Díaz, R. M. Blanco, M. Sánchez-Sánchez and C. Márquez-Álvarez, ed. V. Blay, L. F. Bobadilla and A. Cabrera García, *Zeolites and Metal-Organic Frameworks - From lab to industry*, Amsterdam University Press, 2018, pp. 149–174.

7 R. Zubrzycki and T. Ressler, *Microporous Mesoporous Mater.*, 2015, **214**, 8–14.

8 N. Rahmat, A. Z. Abdullah and A. R. Mohamed, *Am. J. Appl. Sci.*, 2010, **7**, 1579–1586.

9 T. M. Albayati, I. K. Salih and H. F. Alazzawi, *Heliyon*, 2019, **5**, e02539.

10 A.-M. Putz, A. Policicchio, S. Stelitano, P. Sfîrloagă, C. Ianăşi, R. G. Agostino and S. Cecilia, *Fullerenes, Nanotubes Carbon Nanostruct.*, 2018, **26**, 810–819.

11 R. Guillet-Nicolas, F. Bérubé, M. Thommes, M. T. Janicke and F. Kleitz, *J. Phys. Chem. C*, 2017, **121**, 24505–24526.

12 J. S. Lettow, Y. J. Han, P. Schmidt-Winkel, P. Yang, D. Zhao, G. D. Stucky and J. Y. Ying, *Langmuir*, 2000, **16**, 8291–8295.

13 P. Schmidt-Winkel, W. W. Lukens, P. Yang, D. I. Margolese, J. S. Lettow, J. Y. Ying and G. D. Stucky, *Chem. Mater.*, 2000, **12**, 686–696.

14 D. Desplantier-Giscard, A. Galarneau, F. Di Renzo and F. Fajula, in *Studies in Surface Science and Catalysis: Zeolites and Mesoporous Materials at the Dawn of the 21st Century*, ed. A. Galarneau, F. Fajula, F. Di Renzo and J. Vedrine, Elsevier, 2001, vol. 135, p. 205.

15 O. Daoura, S. Daher, M.-N. Kaydouh, N. El Hassan, P. Massiani, F. Launay and M. Boutros, *Int. J. Hydrogen Energy*, 2018, **43**, 17205–17215.

16 P.-C. Kuo, Z.-X. Lin, T.-Y. Wu, C.-H. Hsu, H.-P. Lin and T.-S. Wu, *RSC Adv.*, 2021, **11**, 10010–10017.

17 L. Huang and M. Kruk, *Chem. Mater.*, 2015, **27**, 679–689.

18 M. Kruk, *Acc. Chem. Res.*, 2012, **45**, 1678–1687.

19 Y. Awoke, Y. Chebude and I. Díaz, *Molecules*, 2020, **25**, 4909.

20 C. Gérardin, J. Reboul, M. Bonne and B. Lebeau, *Chem. Soc. Rev.*, 2013, **42**, 4217–4255.

21 A. Galarneau, F. Sartori, M. Cangiotti, T. Mineva, F. Di Renzo and M. F. Ottaviani, *J. Phys. Chem. B*, 2010, **114**, 2140–2152.

22 A. G. Kong, H. W. Wang, Z. He, H. M. Ding and Y. K. Shan, *Mater. Lett.*, 2008, **62**, 2973–2976.

23 P. Botella, A. Corma and M. Quesada, *J. Mater. Chem.*, 2012, **22**, 6394–6401.

24 Z. Moradi and A. Ghorbani-Choghamarani, *RSC Adv.*, 2023, **13**, 2265–2268.

25 Z. Gao and I. Zharov, *Chem. Mater.*, 2014, **26**, 2030–2037.

26 C. P. Canlas and T. J. Pinnavaia, *RSC Adv.*, 2012, **2**, 7449–7455.

27 M. Ulfa, D. Prasetyoko, W. Trisunaryanti, H. Bahruji, Z. A. Fadila and N. A. Sholeha, *Sci. Rep.*, 2022, **12**, 15271.

28 N. Baccile, N. Nassif, L. Malfatti, I. N. A. van Bogaert, W. Soetaert, G. Pehau-Arnaudet and F. Babonneau, *Green Chem.*, 2010, **12**, 1564–1567.

29 G. Feng, J. Wang, M. Boronat, Y. Li, J.-H. Su, J. Huang, Y. Ma and J. Yu, *J. Am. Chem. Soc.*, 2018, **140**, 4770–4773.

30 M. Virot, V. Tomao, C. Ginies, F. Visinoni and F. Chemat, *J. Chromatogr. A*, 2008, **1196–1197**, 147–152.

31 M. A. Martin-Luengo, M. Yates, E. S. Rojo, D. Huerta Arribas, D. Aguilar and E. Ruiz Hitzky, *Appl. Catal., A*, 2010, **387**, 141–146.

32 P. Bajpai, in *Biermann's Handbook of Pulp and Paper*, ed. P. Bajpai, Elsevier, 3rd edn, 2018, pp. 363–371.

33 European Chemicals Agency, *Candidate List of Substances of Very High Concern for Authorisation*, 2023, available at, **https://echa.europa.eu/candidate-list-table**, accessed January 2023.

34 B. W. Brooks, *Green Chem.*, 2019, **21**, 2575–2582.

35 P. T. Anastas and J. C. Warner, *Green Chemistry: Theory and Practice*, Oxford University Press, New York, 1998.

36 M. Thommes, K. Kaneko, A. V. Neimark, J. P. Olivier, F. Rodriguez-Reinoso, J. Rouquerol and K. S. Sing, *Pure Appl. Chem.*, 2015, **87**, 1051–1069.

37 C. Schlumberger and M. Thommes, *Adv. Mater. Interfaces*, 2021, **8**, 2002181.

38 M. Thommes, B. Smarsly, M. Groenewolt, P. I. Ravikovitch and A. V. Neimark, *Langmuir*, 2006, **22**, 756–764.

39 H. I. Lee, J. H. Kim, G. D. Stucky, Y. Shi, C. Pak and J. M. Kim, *J. Mater. Chem.*, 2010, **20**, 8483–8487.

40 S. Maiti, A. André, S. Maiti, M. Hodas, M. Jankowski, M. Scheele and F. Schreiber, *J. Phys. Chem. Lett.*, 2019, **10**, 6324–6330.

41 M. Kruk, M. Jaroniec, C. H. Ko and R. Ryoo, *Chem. Mater.*, 2000, **12**, 1961–1968.

42 UNE EN ISO 14044:2006/A1:2018, *Environmental Management – Life Cycle Assessment – Requirements and Guidlines*, Beuth, 2018.

43 ESU-Services Ltd., *Life Cycle Assessment of Orange Juice Harmonised Environmental Sustainability in the European Food and Drink Chain*, 2013, available at, **https://esu-services.ch/fileadmin/download/doublet-2013-SENSE_Deliverable-2_1-LCAorangejuice.pdf**.

44 R. Heijungs and J. B. Guinée, *J. Waste Manag.*, 2007, **27**, 997–1005.

45 *US Pat.*, 7157397B2, 2004.

46 V. M. Zakoshansky, *Pet. Chem.*, 2007, **47**, 273–284.

47 W. Klöpffer and B. Grahl, *Life Cycle Assessment (LCA): A Guide to Best Practice*, John Wiley & Sons, Ltd, 2014.

48 M. G. Hipolito, *Life Cycle Assessment of Platform Chemicals from Fossil and Lignocellulosic Biomass Scenarios: Phenolic Compounds, Solvent, Soft and Hard Plastic Precursors*, Lambert Academic Publishing, 2011.

49 R. Ciriminna, M. Lomeli-Rodriguez, P. Demma Carà, J. A. Lopez-Sanchez and M. Pagliaro, *Chem. Commun.*, 2014, **50**, 15288–15296.

50 W. Widmer, W. Zhou and K. Grohmann, *Bioresour. Technol.*, 2010, **101**, 5242–5249.

51 M. Pourbafrani, G. Forgács, I. S. Horváth, C. Niklasson and M. J. Taherzadeh, *Bioresour. Technol.*, 2010, **101**, 4246–4250.

52 K. Grohmann, R. G. Cameron and B. S. Buslig, *Bioresour. Technol.*, 1995, **54**, 129–141.

53 W. Zhou, W. W. Widmer and K. Grohmann, *Proc. Fla. State Hortic. Soc.*, 2007, **120**, 310–315.

54 F. R. Alvarez, G. M. Shaul, E. R. Krishnan, D. L. Perrin and M. Rahman, *J. Air Waste Manage. Assoc.*, 1999, **49**, 734–739.

55 I. John, K. Muthukumar and A. Arunagiri, *Int. J. Green Energy*, 2017, **14**, 599–612.

56 International Energy Agency, *World Energy Balances*, 2022, available at, **https://www.iea.org/data-and-statistics/data-product/world-energy-balances**.

57 UNECE, *Carbon Neutrality in the UNECE Region: Integrated Life-cycle Assessment of Electricity Sources*, 2021, available at, **https://unece.org/sites/default/files/2022-04/LCA_3_FINAL_March_2022.pdf**.

58 F. Asdrubali, G. Baldinelli, F. D'Alessandro and F. Scrucca, *Renewable Sustainable Energy Rev.*, 2015, **42**, 1113–1122.

59 M. Zhu, J. Sun, Y. Tian, M. Ren and X. Li, *Asia-Pac. J. Chem. Eng.*, 2007, **2**, 278–281.

60 S. A. Matlin, S. E. Cornell, A. Krief, H. Hopf and G. Mehta, *Chem. Sci.*, 2022, **13**, 11710–11720.

61 I. Schuldes, D. M. Noll, T. Schindler, T. Zech, K. Götz, M.-S. Appavou, P. Boesecke, F. Steiniger, P. S. Schulz and T. Unruh, *Langmuir*, 2019, **35**, 13578–13587.

62 T. Kassar, N. S. Güldal, M. Berlinghof, T. Ameri, A. Kratzer, B. C. Schroeder, G. L. Destri, A. Hirsch, M. Heeney, I. McCulloch, C. J. Brabec and T. Unruh, *Adv. Energy Mater.*, 2016, **6**, 1502025.

63 M. A. J. Huijbregts, Z. J. N. Steinmann, P. M. F. Elshout, G. Stam, F. Verones, M. Vieira, M. Zijp, A. Hollander and R. van Zelm, *Int. J. Life Cycle Assess.*, 2017, **22**, 138–147.

64 E. R. Monteith, P. Mampuys, L. Summerton, J. H. Clark, B. U. W. Maes and C. R. McElroy, *Green Chem.*, 2020, **22**, 123–135.

65 C. R. McElroy, A. Constantinou, L. C. Jones, L. Summerton and J. H. Clark, *Green Chem.*, 2015, **17**, 3111–3121.

66 C. Jimenez-Gonzalez, C. S. Ponder, Q. B. Broxterman and J. B. Manley, *Org. Process Res. Dev.*, 2011, **15**, 912–917.